# Energetic BEM–FEM coupling for wave propagation in 3D multidomains

A. Aimi[1,*,†], M. Diligenti[1], A. Frangi[2] and C. Guardasoni[1]

[1]*Department of Mathematics and Computer Science, University of Parma, Parma, Italy*
[2]*DICA, Politecnico of Milano, Milan, Italy*

## 1. INTRODUCTION

Time-dependent problems modelled by hyperbolic PDEs can be formulated in terms of boundary integral equations (BIEs) and solved via the Boundary Element Method (BEM). Successful applications have been demonstrated, for example, in seismology, in particular for the analysis of soil-structure interaction, in acoustic, and in the scattering of electromagnetic waves (see, e.g. [1–3]).

The BEM, also when formulated directly in the space–time domain, has attracted particular interest for various reasons, which among others are its high accuracy, the implicit fulfilment of the radiation conditions at infinity, the low cost of discretization when problems are defined over unbounded domains, the simplicity of imposing the interface conditions in problems defined on multidomains since the continuity and compatibility conditions that have to be satisfied on the interface respectively by the primal unknown function and its derivative can be simply incorporated because they both appear directly in the boundary integral formulation.

However, one can identify a number of situations where complicated structural features or nonlinear phenomena can be localized in small parts of an otherwise infinite and linear domain. Examples are provided by regions having nonhomogeneous material properties (e.g. layered soils, [4,5]), constitutive nonlinearities (e.g. elastoplasticity [6]), evolving topology (e.g. linear fracture mechanics [7]) or even different physics (e.g. in solid–fluid coupling [8] or wave–soil–structure interaction [9]). In these contexts, the BEM should be understood as complementary rather than concurrent to standard domain approaches like a general purpose FEM. It should be further stressed that, in many applications to time-dependent problems, a domain method requires to truncate the discretization at some distance from the region of interest. In order to avoid spurious wave reflections, specific provisions must be adopted on the truncation surface, such as absorbing boundary conditions (ABCs)

---

*Correspondence to: A. Aimi, Department of Mathematics and Computer Science, University of Parma, Parco Area delle Scienze, 53/A, 43124 Parma, Italy.
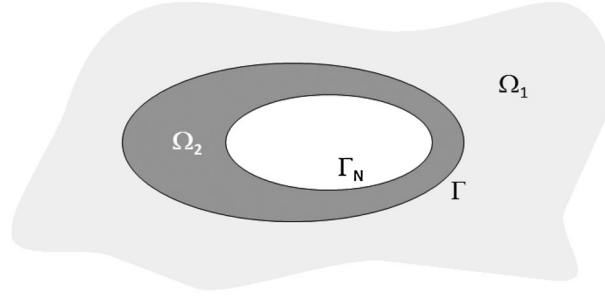
†E-mail: alessandra.aimi@unipr.it

Figure 1. Transversal section of the spatial domain for the model problem.

or perfectly matched layers (see, e.g. the comparative analysis in [10]). However, these techniques still suffer from many drawbacks which, on the contrary, could be brilliantly solved by coupling the FEM with the BEM (a very recent contribution in this direction can be found in [11]).

In the last decades, contributions to BEM–FEM coupling, in the context of hyperbolic problems, started to appear [12–16], especially analyzing stability issues. However, if the classical BEM is employed, the range of applicable time step lengths resulting in a stable and accurate solution is limited. Indeed, accuracy and stability considerations of both the BEM itself and the FEM might impose requirements on the choice of the time step durations, which may be contradictory (see, e.g. [17]). This issue has somehow limited new developments. On the contrary, in this work, we start from a recently developed energetic space–time weak formulation of BIEs related to wave propagation problems defined on single and multidomains (see in particular [18–21] and references therein). This technique has shown excellent stability properties, which are crucial in guaranteeing an efficient coupling with the FEM.

As a consequence, in this investigation, we present a coupling algorithm, which allows a flexible use of FEM and BEM as local discretization techniques, in order to efficiently treat bounded or unbounded multidomains. PDEs associated to BIEs will be weakly reformulated by the energetic approach, and a particular emphasis will be given to theoretical and experimental analyses of the stability of the proposed method. The paper is structured as follows: in Sections 2 and 3, the model problem and its energetic weak formulation are introduced; Section 4 is dedicated to the Galerkin BEM–FEM discretization phase. Energy estimates for the numerical scheme are proved in Section 5 and extensions of the model problem are detailed in Section 6. In Section 7, several numerical results are presented and discussed before the conclusive Section, which summarizes the main features of the energetic coupling approach and outlines future investigations.

## 2. MODEL PROBLEM

Let $\Omega \subset \mathbb{R}^3$ be an open bounded domain, with a sufficiently smooth boundary $\Gamma_N := \partial\Omega$. Let $\Omega_1 \cup \Omega_2 = \mathbb{R}^3 \setminus \Omega$ be a decomposition of $\mathbb{R}^3 \setminus \Omega$, with $\Omega_1$ unbounded and $\Omega_2$ bounded nonoverlapping subdomains such that $\bar{\Omega}_1 \cap \bar{\Omega} = \emptyset$ and $\bar{\Omega}_1 \cap \bar{\Omega}_2 = \Gamma$, as illustrated in Figure 1. It should be remarked that the boundary of the unbounded subdomain $\Omega_1$ reduces to the interface $\Gamma$. We denote by $u_i(\mathbf{x}, t)$, hereafter called pressure, the unknown function in the $i$-th subdomain and by $p_i(\mathbf{x}, t) := \mu_i(\partial u_i / \partial\mathbf{n}_\mathbf{x})(\mathbf{x}, t)$, called traction, the normal gradient of pressure, where $\mathbf{n}_\mathbf{x}$ is the unit (outward) normal vector and $\mu_i$ is a material parameter for the subdomain $\Omega_i$.

Let us now consider the following wave propagation model problem:

$$\Delta u_i(\mathbf{x}, t) - (1/c_i^2)\ddot{u}_i(\mathbf{x}, t) = f_i(\mathbf{x}, t), \quad \mathbf{x} \in \Omega_i, \, t \in [0, T], \, i = 1, 2 \tag{1}$$

$$u_i(\mathbf{x}, 0) = 0, \quad \mathbf{x} \in \Omega_i, \, i = 1, 2 \tag{2}$$

$$\dot{u}_i(\mathbf{x}, 0) = 0, \quad \mathbf{x} \in \Omega_i, \, i = 1, 2 \tag{3}$$

$$p_2(\mathbf{x}, t) = \bar{p}(\mathbf{x}, t), \quad \mathbf{x} \in \Gamma_N, \, t \in [0, T], \tag{4}$$

$$u_1(\mathbf{x}, t) = u_2(\mathbf{x}, t), \, p_1(\mathbf{x}, t) = -p_2(\mathbf{x}, t), \quad \mathbf{x} \in \Gamma, \, t \in [0, T], \tag{5}$$

where dots denote derivatives with respect to time, $c_i$ is the propagation velocity of a perturbation in the $i$-th subdomain, $\bar{p}(\mathbf{x},t)$ is a given function, the assigned PDE right-hand sides $f_1(\mathbf{x},t) \equiv 0$ and $f_2(\mathbf{x},t)$ are suitably connected and the continuity and equilibrium conditions (5) for the solutions are imposed at the interface $\Gamma$ between the two subdomains.

The unknown functions $u_i$ are understood in a weak sense, i.e. $u_i \in H^1([0,T]; H^1(\Omega_i))$. Because the goal of this work is to approximate $u_1$ using a BEM approach and $u_2$ using a FEM technique, we have to obtain a boundary integral reformulation of the problem (1)–(5) in $\Omega_1$.

Let us consider the boundary integral representation of $u_1(\mathbf{x},t)$, for $\mathbf{x} \in \Omega_1, t \in [0,T]$:

$$u_1(\mathbf{x},t) = \frac{1}{\mu_1} \int_\Gamma \int_0^t G(r,t-\tau) p_1(\boldsymbol{\xi},\tau) d\tau \, d\gamma_{\boldsymbol{\xi}} - \int_\Gamma \int_0^t \frac{\partial G}{\partial \mathbf{n}_{\boldsymbol{\xi}}}(r,t-\tau) u_1(\boldsymbol{\xi},\tau) \, d\tau \, d\gamma_{\boldsymbol{\xi}}, \quad (6)$$

where $r = \|\mathbf{r}\|_2 = \|\mathbf{x} - \boldsymbol{\xi}\|_2$ and

$$G(r,t-\tau) = \frac{c_1}{4\pi r} \delta[c_1(t-\tau)-r] \quad (7)$$

is the forward fundamental solution of the three-dimensional wave operator, with $\delta[\cdot]$ as the Dirac distribution.

Differentiating (6) with respect to $t$ and performing a limiting process for $\mathbf{x}$ tending to $\Gamma$, we obtain the so-called *velocity* BIE [22],

$$\frac{1}{2}\dot{u}_1(\mathbf{x},t) = \frac{1}{\mu_1}(V\dot{p}_1)(\mathbf{x},t) - (K\dot{u}_1)(\mathbf{x},t). \quad (8)$$

where

$$Vp_1(\mathbf{x},t) = \int_\Gamma \int_0^t G(r,t-\tau)p_1(\boldsymbol{\xi},\tau)\,d\tau\,d\gamma_{\boldsymbol{\xi}} \quad (9)$$

and

$$Ku_1(\mathbf{x},t) = \int_\Gamma \int_0^t \frac{\partial G}{\partial \mathbf{n}_{\boldsymbol{\xi}}}(r,t-\tau)u_1(\boldsymbol{\xi},\tau)\,d\tau\,d\gamma_{\boldsymbol{\xi}} \quad (10)$$

$$= -\int_\Gamma \frac{\partial r}{\partial \mathbf{n}_{\boldsymbol{\xi}}} \int_0^t G(r,t-\tau)\left[\frac{\dot{u}_1(\boldsymbol{\xi},\tau)}{c_1} + \frac{u_1(\boldsymbol{\xi},\tau)}{r}\right] d\tau\,d\gamma_{\boldsymbol{\xi}}.$$

Taking into account the presence of the Dirac distribution in the kernels of the aforementioned boundary integral operators $V$ and $K$, the time integration can be performed analytically yielding the following final simplified expressions:

$$Vp_1(\mathbf{x},t) = \int_\Gamma \frac{1}{4\pi r} H[t - \frac{r}{c_1}] p_1(\boldsymbol{\xi},t-\frac{r}{c_1})\,d\gamma_{\boldsymbol{\xi}}, \quad (11)$$

$$Ku_1(\mathbf{x},t) = -\int_\Gamma \frac{1}{4\pi r} H[t-\frac{r}{c_1}]\frac{\partial r}{\partial \mathbf{n}_{\boldsymbol{\xi}}}\left[\frac{\dot{u}_1(\boldsymbol{\xi},t-\frac{r}{c_1})}{c_1} + \frac{u_1(\boldsymbol{\xi},t-\frac{r}{c_1})}{r}\right] d\gamma_{\boldsymbol{\xi}}, \quad (12)$$

where $H[\cdot]$ is the Heaviside function.

Now, if we derive with respect to time the expressions (11) and (12), after a straightforward computation, we obtain

$$(V\dot{p}_1)(\mathbf{x},t) = (V\dot{p}_1)(\mathbf{x},t), \quad (K\dot{u}_1)(\mathbf{x},t) = (K\dot{u}_1)(\mathbf{x},t). \quad (13)$$

Inserting (13) into the BIE (8), we can conclude that problems (1)–(5) in the subdomain $\Omega_1$ can be rewritten as the following space–time BIE in the boundary unknowns $p_1(\mathbf{x},t)$ and $u_1(\mathbf{x},t)$ on $\Gamma$:

$$\frac{1}{2}\dot{u}_1(\mathbf{x},t) = \frac{1}{\mu_1}(V\dot{p}_1)(\mathbf{x},t) - (K\dot{u}_1)(\mathbf{x},t). \quad (14)$$

Of course, this problem has to be coupled with the differential one specified for $\Omega_2$, under the coupling conditions (5) at the interface. In particular, here, we are interested in a direct space–time weak formulation for the coupling of the integro-differential problem on $\Omega_1 \cup \Omega_2$, and this will be done in the next section.

## 3. ENERGETIC WEAK FORMULATION FOR THE COUPLING

We start remarking that the solution of (1)–(5) in $\Omega_1$ satisfies the following energy identity:

$$\mathcal{E}_{\Omega_1}(u_1, T) := \frac{1}{2} \int_{\Omega_1} \left[ \frac{1}{c_1^2} \dot{u}_1^2(\mathbf{x}, T) + |\nabla u_1(\mathbf{x}, T)|^2 \right] d\mathbf{x}\, dt = \frac{1}{\mu_1} \int_{\Gamma} \int_0^T \dot{u}_1(\mathbf{x}, t) p_1(\mathbf{x}, t)\, dt\, d\gamma_{\mathbf{x}} \tag{15}$$

which can be obtained by multiplying with $\dot{u}_1$ Equation (1) specified for $i = 1$ and integrating by parts over $\Omega_1 \times [0, T]$.

Then, taking into account the nature of Equation (14), its *energetic* weak formulation is defined as follows:

find $u_1 \in H^1([0, T]; H^{\frac{1}{2}}(\Gamma))$ and $p_1 \in L^2([0, T]; H^{-\frac{1}{2}}(\Gamma))$ such that

$$\frac{1}{2} < \dot{u}_1, q_1 >= \frac{1}{\mu_1} < V\dot{p}_1, q_1 > - < K\dot{u}_1, q_1 >, \quad \forall q_1 \in L^2([0, T]; H^{-\frac{1}{2}}(\Gamma)), \tag{16}$$

where $< \cdot, \cdot >=< \cdot, \cdot >_{L^2([0,T]\times\Gamma)}$.

For the energetic weak formulation in $\Omega_2$, let us multiply the differential Equation (1), specified for $i = 2$, for the time derivative of test functions $v_2 \in H^1([0, T]; H^1(\Omega_2))$ and integrate by parts in space obtaining, after a multiplication by the coefficient $\mu_2$:

$$-\mu_2 \mathcal{A}(u_2, v_2) + < p_{2|\Gamma}, \dot{v}_{2|\Gamma} >= \mu_2 \mathcal{F}(v_2) - < \bar{p}, \dot{v}_{2|\Gamma_N} >_{\Gamma_N}, \tag{17}$$

where

$$\mathcal{A}(u_2, v_2) := \int_0^T \int_{\Omega_2} \left[ \nabla \dot{v}_2(\mathbf{x}, t) \cdot \nabla u_2(\mathbf{x}, t) + \frac{1}{c_2^2} \dot{v}_2(\mathbf{x}, t)\, \ddot{u}_2(\mathbf{x}, t) \right] d\mathbf{x}\, dt, \tag{18}$$

$$\mathcal{F}(v_2) := \int_0^T \int_{\Omega_2} \dot{v}_2(\mathbf{x}, t) f_2(\mathbf{x}, t)\, d\mathbf{x}\, dt \tag{19}$$

and $< \cdot, \cdot >_{\Gamma_N} =< \cdot, \cdot >_{L^2([0,T]\times\Gamma_N)}$.

Now, remembering the interface conditions (5), we finally obtain the following energetic weak formulation of the coupled problem

$$\begin{cases} \frac{1}{\mu_1} < V\dot{p}_1, q_1 > - < K\dot{u}_{2|\Gamma}, q_1 > -\frac{1}{2} < \dot{u}_{2|\Gamma}, q_1 >= 0, & \forall q_1 \in L^2([0, T]; H^{-\frac{1}{2}}(\Gamma)) \\ \mu_2 \mathcal{A}(u_2, v_2) + < p_1, \dot{v}_{2|\Gamma} >= -\mu_2 \mathcal{F}(v_2) + < \bar{p}, \dot{v}_{2|\Gamma_N} >_{\Gamma_N}, & \forall v_2 \in H^1([0, T]; H^1(\Omega_2)) \end{cases}. \tag{20}$$

At every time instant, the unknowns are $p_1$ over the interface $\Gamma$ and $u_2$ in $\bar{\Omega}_2$. Further, let us note that in the particular case $\mu_1 = \mu_2$ and $c_1 = c_2$, the first equation in (20) can be regarded as a weak ABC to reduce an unbounded domain to a computational bounded one, avoiding spurious incoming reflections: this property will be shown in Section 7 by means of several numerical results.

Let us conclude this section with some energy considerations. Choosing $v_2 = u_2$, in (18), one gets

$$\mathcal{A}(u_2, u_2) = \mathcal{E}_{\Omega_2}(u_2, T). \tag{21}$$

With the same choice for the second equations in (20), which involves all the problem unknowns, and remembering (15), the following relation appears

$$\mu_1 \mathcal{E}_{\Omega_1}(u_1, T) + \mu_2 \mathcal{E}_{\Omega_2}(u_2, T) = -\mu_2 \mathcal{F}(u_2) + < \bar{p}, \dot{u}_{2|\Gamma_N} >_{\Gamma_N}, \tag{22}$$

from which one can deduce *a priori* stability estimates for regular solutions.

## 4. SPACE–TIME GALERKIN DISCRETIZATION

For time discretization, we consider a uniform decomposition of the time interval $[0, T]$ with time step $\Delta t = T/N_{\Delta t}$, $N_{\Delta t} \in \mathbb{N}^+$, generated by the $N_{\Delta t} + 1$ time-knots

$$t_k = k\,\Delta t, \quad k = 0, \cdots, N_{\Delta t},$$

and we choose piecewise constant shape functions for the time approximation of $p$ and piecewise linear shape functions for the time approximation of $u$ although higher-degree shape functions can be used. In particular, time shape functions, for $k = 0, \cdots, N_{\Delta t} - 1$, will be defined as

$$\bar{\psi}_k(t) = H[t - t_k] - H[t - t_{k+1}] \tag{23}$$

for the approximation of $p_1$ and as

$$\hat{\psi}_k(t) = R(t - t_k) - R(t - t_{k+1}), \tag{24}$$

for the approximation of $u_2$, where $R(t - t_k) = \frac{t - t_k}{\Delta t} H[t - t_k]$ is the ramp function.

For the space discretization, we consider the bounded subdomain $\Omega_2$ (suitably approximated by a domain of polyhedral type) and a mesh $\mathcal{T}_{\Omega_2, \Delta x} = \{e_1, \cdots, e_{M_{\Delta x}}\}$ constituted by $M_{\Delta x}$ tetrahedra, with $diam(e_i) \leq \Delta x$, $e_i \cap e_j = \emptyset$ if $i \neq j$ and such that $\bigcup_{i=1}^{M_{\Delta x}} \overline{e}_i = \overline{\Omega}_2$. The mesh $\mathcal{T}_{\Gamma, \Delta x}$ on the interface will be the restriction of $\mathcal{T}_{\Omega_2, \Delta x}$ to $\Gamma$ and therefore the collection of $M_\Gamma$ nonoverlapping triangles.

The functional background compels one to choose spatially shape functions belonging to $L^2(\Gamma)$ for the approximation of $p$ and to $C^0(\Omega_2)$ for the approximation of $u$. Hence, we will choose piecewise constant basis functions $\bar{\varphi}_j(\mathbf{x})$, $j = 1, \cdots, M_\Gamma$ related to $\mathcal{T}_{\Gamma, \Delta x}$ for the approximation of $p$ over the interface and piecewise linear continuous functions $\hat{\varphi}_j(\mathbf{x})$, $j = 1, \cdots, M_{\Omega_2}$ related to $\mathcal{T}_{\Omega_2, \Delta x}$ for the approximation of $u$ in $\Omega_2$. The approximate solutions of the problem at hand will be expressed as

$$p_1(\mathbf{x}, t) \simeq \sum_{k=0}^{N_{\Delta t}-1} \bar{\psi}_k(t) \bar{\Phi}_k(\mathbf{x}) := \sum_{k=0}^{N_{\Delta t}-1} \bar{\psi}_k(t) \sum_{j=1}^{M_\Gamma} \bar{\alpha}_{kj}\, \bar{\varphi}_j(\mathbf{x}), \tag{25}$$

$$u_2(\mathbf{x}, t) \simeq \sum_{k=0}^{N_{\Delta t}-1} \hat{\psi}_k(t) \hat{\Phi}_k(\mathbf{x}) := \sum_{k=0}^{N_{\Delta t}-1} \hat{\psi}_k(t) \sum_{j=1}^{M_{\Omega_2}} \hat{\alpha}_{kj}\, \hat{\varphi}_j(\mathbf{x}). \tag{26}$$

The Galerkin BEM–FEM discretization coming from energetic weak formulation (16) produces the linear system

$$\mathbb{E}\,\boldsymbol{\alpha} = \mathbf{b}, \tag{27}$$

where matrix $\mathbb{E}$ has a block lower triangular Toeplitz structure, because its elements depend on the difference $\Delta_{hk} := t_h - t_k$, and in particular, they vanish if $t_h < t_k$. Each block has dimensions $M := M_\Gamma + M_{\Omega_2}$. If we denote by $\mathbb{E}^{(\ell)}$ the block obtained when $\Delta_{hk} = \ell\,\Delta t$, $\ell = 0, \ldots, N_{\Delta t} - 1$, the linear system can be written as

$$\begin{pmatrix}
\mathbb{E}^{(0)} & 0 & 0 & \cdots & 0 \\
\mathbb{E}^{(1)} & \mathbb{E}^{(0)} & 0 & \cdots & 0 \\
\mathbb{E}^{(2)} & \mathbb{E}^{(1)} & \mathbb{E}^{(0)} & \cdots & 0 \\
\cdots & \cdots & \cdots & \cdots & 0 \\
\mathbb{E}^{(N_{\Delta t}-1)} & \mathbb{E}^{(N_{\Delta t}-2)} & \cdots & \mathbb{E}^{(1)} & \mathbb{E}^{(0)}
\end{pmatrix}
\begin{pmatrix}
\boldsymbol{\alpha}^{(0)} \\
\boldsymbol{\alpha}^{(1)} \\
\boldsymbol{\alpha}^{(2)} \\
\vdots \\
\boldsymbol{\alpha}^{(N_{\Delta t}-1)}
\end{pmatrix}
=
\begin{pmatrix}
\mathbf{b}^{(0)} \\
\mathbf{b}^{(1)} \\
\mathbf{b}^{(2)} \\
\vdots \\
\mathbf{b}^{(N_{\Delta t}-1)}
\end{pmatrix} \tag{28}$$

where

$$\boldsymbol{\alpha}^{(\ell)} = \left(\alpha_j^{(\ell)}\right), \quad \mathbf{b}^{(\ell)} = \left(b_j^{(\ell)}\right), \quad \ell = 0, \ldots, N_{\Delta t} - 1; \; j = 1, \ldots, M,$$

and the unknowns are organized as follows:

$$\boldsymbol{\alpha}^{(\ell)} = \left( \bar{\alpha}_{\ell\,1}, \cdots, \bar{\alpha}_{\ell\,M_\Gamma}, \hat{\alpha}_{\ell\,1}, \cdots, \hat{\alpha}_{\ell\,M_{\Omega_2}} \right)^\top .$$

Note that each block has a symmetric $2 \times 2$ block substructure of the type

$$\mathbb{E}^{(\ell)} = \begin{bmatrix} \mathbb{E}_\Gamma^{(\ell)} & \mathbb{E}_{\Gamma,FEM}^{(\ell)} \\ \mathbb{E}_{FEM,\Gamma}^{(\ell)} & \mathbb{E}_{FEM}^{(\ell)} \end{bmatrix} \tag{29}$$

where we can recognize the contribution of the coupling on the interface $\Gamma$ and of the pure energetic FEM inside $\Omega_2$, and it presents a highly sparse structure.

The solution of (28) is obtained with a block forward substitution, that is, at every time instant $t_\ell = \ell\,\Delta t$, $\ell = 0, \cdots, N_{\Delta t} - 1$, one computes

$$\mathbf{z}^{(\ell)} = \mathbf{b}^{(\ell)} - \sum_{j=1}^\ell \mathbb{E}^{(j)} \boldsymbol{\alpha}^{(\ell-j)}$$

and then solves the reduced linear system

$$\mathbb{E}^{(0)} \boldsymbol{\alpha}^{(\ell)} = \mathbf{z}^{(\ell)} . \tag{30}$$

Procedure (30) is a time-marching technique, where the only matrix to be inverted is the nonsingular block $\mathbb{E}^{(0)}$; therefore, the $LU$ factorization needs to be performed only once and saved. At each time step, the solution of (30) requires only forward and backward substitution phases, whereas all the other blocks are used to update at every time step the right-hand side. Owing to this procedure, we can construct and store only the blocks $\mathbb{E}^{(0)}, \cdots, \mathbb{E}^{(N_{\Delta t}-1)}$, with a considerable reduction of computational cost and memory requirement.

Now, referring to the left-hand sides of the weak problem (20), after an analytic integration in the time variable, we have the following results.

Matrix elements coming from the discretization of $< V \dot{p}_1, q_1 >$ are of the form

$$-\frac{1}{4\pi} \sum_{\alpha,\beta=0}^1 (-1)^{\alpha+\beta} \int_\Gamma \bar{\varphi}_i(\mathbf{x}) \int_\Gamma \frac{1}{r} H[\Delta_{h+\alpha,k+\beta} - \frac{r}{c_1}] \bar{\varphi}_j(\boldsymbol{\xi})\, d\gamma_{\boldsymbol{\xi}}\, d\gamma_{\mathbf{x}}, \tag{31}$$

whereas matrix elements coming from the discretization of $< K \dot{u}_{2|\Gamma}, q_1 >$ are of the form

$$-\frac{1}{4\pi\Delta t} \sum_{\alpha,\beta=0}^1 (-1)^{\alpha+\beta} \Delta_{h+\alpha,k+\beta} \int_\Gamma \bar{\varphi}_i(\mathbf{x}) \int_\Gamma \frac{1}{r} H[\Delta_{h+\alpha,k+\beta} - \frac{r}{c_1}] \frac{\mathbf{r} \cdot \mathbf{n}_{\boldsymbol{\xi}}}{r^2} \hat{\varphi}_{j\,|\Gamma}(\boldsymbol{\xi})\, d\gamma_{\boldsymbol{\xi}}\, d\gamma_{\mathbf{x}}. \tag{32}$$

We observe in (31) and (32) space singularities of type $O(r^{-1})$ as $r \to 0$, which are typical of weakly singular kernels related to 3D elliptic problems, and also the presence of the Heaviside function, which analytically represents the wave front propagation. We refer the interested reader to [20, 21] for the description of the accurate and fast evaluation of such types of double integrals on the interface $\Gamma$. Further, it is simple to prove that, because of the chosen time basis functions, expressions (31) and (32) vanish for $\ell$ such that $t_\ell \geq diam\left(\Omega \bigcup \Omega_2\right)/c_1 + \Delta t$; this cut-off property is important to drastically decrease the computation of the time-marching procedure, especially in the context of 3D problems.

For what concerns matrix elements coming from $< \dot{u}_{2|\Gamma}, q_1 >$, one has

$$\delta_{hk} \int_\Gamma \hat{\varphi}_{j\,|\Gamma}(\mathbf{x})\, \bar{\varphi}_i(\mathbf{x})\, d\gamma_{\mathbf{x}}, \tag{33}$$

where $\delta_{hk}$ is the Kronecker symbol. An analogous result holds for the discretization of $< p_1, \dot{v}_{2|\Gamma} >$.

Finally, matrix elements coming from $\mathcal{A}(v_2, u_2)$ will be of the type

$$\varrho_{hk} \int_{\Omega_2} \nabla \hat{\varphi}_j(\mathbf{x}) \cdot \nabla \hat{\varphi}_i(\mathbf{x}) \, d\gamma_{\mathbf{x}} + \frac{1}{c_2^2} \frac{\eta_{hk}}{(\Delta t)^2} \int_{\Omega_2} \hat{\varphi}_j(\mathbf{x}) \, \hat{\varphi}_i(\mathbf{x}) \, d\gamma_{\mathbf{x}}, \tag{34}$$

where

$$\varrho_{hk} = \begin{cases} \frac{1}{2}, & h = k \\ 1, & h > k \\ 0, & elsewhere \end{cases} \quad \text{and} \quad \eta_{hk} = \begin{cases} 1, & h = k \\ -1, & h = k+1 \\ 0, & elsewhere \end{cases}, \tag{35}$$

Hence, they involve the evaluation of standard stiffness and mass matrices elements related to the bounded subdomain $\Omega_2$.

## 5. ENERGY ESTIMATES FOR THE NUMERICAL SCHEME

Let us consider the second energetic weak equation in (20), which involves all the problem unknowns, and, to simplify the following notation, $\bar{p} = 0$. Now, using (25) and (26) as approximate solutions and $v_2(\mathbf{x}, t) = \dot{\psi}_h(t) \hat{\Phi}_h(\mathbf{x})$ as test function, we obtain

$$\mu_2 \sum_{k=0}^{N_{\Delta t}-1} \left[ (\nabla \hat{\Phi}_h, \nabla \hat{\Phi}_k)_{L^2(\Omega_2)} \int_0^T \dot{\psi}_h(t) \psi_k(t) \, dt + \frac{(\hat{\Phi}_h, \hat{\Phi}_k)_{L^2(\Omega_2)}}{c_2^2} \int_0^T \dot{\psi}_h(t) \ddot{\psi}_k(t) \, dt \right]$$

$$+ \sum_{k=0}^{N_{\Delta t}-1} (\hat{\Phi}_{h|\Gamma}, \bar{\Phi}_k)_{L^2(\Gamma)} \int_0^T \dot{\psi}_h(t) \bar{\psi}_k(t) \, dt = \mu_2 (\hat{\Phi}_h, F_h)_{L^2(\Omega_2)}, \tag{36}$$

where $F_h(\mathbf{x}) = -\int_0^T \dot{\psi}_h(t) \, f_2(\mathbf{x}, t) \, dt$.

Performing analytically time integrals in the left-hand side of (36), we get

$$\mu_2 \sum_{k=0}^{h-1} (\nabla \hat{\Phi}_h, \nabla \hat{\Phi}_k)_{L^2(\Omega_2)} + \frac{\mu_2}{2} (\nabla \hat{\Phi}_h, \nabla \hat{\Phi}_h)_{L^2(\Omega_2)} + \frac{\mu_2}{c_2^2} \left( \hat{\Phi}_h, \frac{\hat{\Phi}_h - \hat{\Phi}_{h-1}}{\Delta t^2} \right)_{L^2(\Omega_2)} \tag{37}$$

$$+ (\hat{\Phi}_{h|\Gamma}, \bar{\Phi}_h)_{L^2(\Gamma)} = \mu_2 (\hat{\Phi}_h, F_h)_{L^2(\Omega_2)}.$$

At this stage, we need to observe that, from (25) and (26),

$$p_1(\mathbf{x}, t_h) \simeq p_1^h := \bar{\Phi}_h(\mathbf{x}), \quad u_2(\mathbf{x}, t_h) \simeq u_2^h := \sum_{k=0}^{h-1} \hat{\Phi}_k(\mathbf{x}); \tag{38}$$

Hence, we can rewrite the numerical scheme (37) as

$$\mu_2 \left( \nabla \left( u_2^{h+1} - u_2^h \right), \nabla \frac{u_2^{h+1} + u_2^h}{2} \right)_{L^2(\Omega_2)} + \frac{\mu_2}{c_2^2} \left( u_2^{h+1} - u_2^h, \frac{u_2^{h+1} - 2 u_2^h + u_2^{h-1}}{\Delta t^2} \right)_{L^2(\Omega_2)}$$

$$+ \left( u_{2|\Gamma}^{h+1} - u_{2|\Gamma}^h, p_1^h \right)_{L^2(\Gamma)} = \mu_2 \left( u_2^{h+1} - u_2^h, F_h \right)_{L^2(\Omega_2)}. \tag{39}$$

*Remark 1*
Here, we want to stress the fact that the proposed energetic weak formulation, after time integration, can be regarded as a Newmark scheme for the differential part of the coupling. In fact, in the first two terms in the left-hand side of (39), we can recognize a semidiscretization in time for the problem in the subdomain $\Omega_2$, operated through the cited technique with parameters $\zeta = \frac{1}{2}$, $\theta = 1$ in the notation of [23]. This particular Newmark scheme is implicit, unconditionally stable and first-order accurate in $\Delta t$.

Now, having set $\| \cdot \| = \| \cdot \|_{L^2(\Omega_i)}$, let us introduce the discrete energy in the subdomain $\Omega_i$, $i = 1, 2$, at the time instant $t_{h+1}$, defined as

$$\mathcal{E}_i^{h+1} := \frac{1}{2} \left[ \frac{1}{c_i^2} \| \frac{u_i^{h+1} - u_i^h}{\Delta t} \|^2 + \| \nabla u_i^{h+1} \|^2 \right];$$
(40)

further, we observe that

$$(\nabla(u_2^{h+1} - u_2^h), \nabla(u_2^{h+1} + u_2^h))_{L^2(\Omega_2)} = \| \nabla u_2^{h+1} \|^2 - \| \nabla u_2^h \|^2$$

and

$$(u_2^{h+1} - u_2^h, u_2^{h+1} - 2 u_2^h + u_2^{h-1})_{L^2(\Omega_2)} = \| u_2^{h+1} - u_2^h \|^2 - (u_2^{h+1} - u_2^h, u_2^h - u_2^{h-1})_{L^2(\Omega_2)}$$

$$\geq \| u_2^{h+1} - u_2^h \|^2 - \frac{1}{2} \| u_2^{h+1} - u_2^h \|^2 - \frac{1}{2} \| u_2^h - u_2^{h-1} \|^2 = \frac{1}{2} \| u_2^{h+1} - u_2^h \|^2 - \frac{1}{2} \| u_2^h - u_2^{h-1} \|^2.$$

Combining these results with (39) and (40), we finally obtain for the discrete energy in the subdomain $\Omega_2$

$$\mu_2 [\mathcal{E}_2^{h+1} - \mathcal{E}_2^h] + (u_{2|\Gamma}^{h+1} - u_{2|\Gamma}^h, p_1^h)_{L^2(\Gamma)} \leq \mu_2 (u_2^{h+1} - u_2^h, F_h)_{L^2(\Omega_2)}.$$
(41)

Now, applying Cauchy–Schwarz inequality to the right-hand side of (41), we get

$$\mu_2 [\mathcal{E}_2^{h+1} - \mathcal{E}_2^h] + (u_{2|\Gamma}^{h+1} - u_{2|\Gamma}^h, p_1^h)_{L^2(\Gamma)} \leq \mu_2 \Delta t \sqrt{2} \| \frac{u_2^{h+1} - u_2^h}{\sqrt{2} c_2 \Delta t} \| \| c_2 F_h \|,$$
(42)

from which, remembering (40), we deduce

$$\mu_2 [\mathcal{E}_2^{h+1} - \mathcal{E}_2^h] + (u_{2|\Gamma}^{h+1} - u_{2|\Gamma}^h, p_1^h)_{L^2(\Gamma)} \leq \mu_2 \Delta t \, \mathcal{E}_2^{h+1} + \mu_2 c_2^2 \frac{\Delta t}{2} \| F_h \|^2.$$
(43)

Let us now sum inequality (43), for $h = 0, \cdots, n - 1$, with $n \leq N_{\Delta t}$, observing that $\mathcal{E}_2^0 = 0$:

$$\mu_2 \mathcal{E}_2^n + \Delta t \sum_{h=0}^{n-1} \left( \frac{u_{2|\Gamma}^{h+1} - u_{2|\Gamma}^h}{\Delta t}, p_1^h \right)_{L^2(\Gamma)} \leq \mu_2 \Delta t \, \mathcal{E}_2^n + \mu_2 \Delta t \sum_{h=0}^{n-1} \mathcal{E}_2^h + \mu_2 c_2^2 \frac{\Delta t}{2} \sum_{h=0}^{n-1} \| F_h \|^2.$$
(44)

Let us note that, remembering the coupling conditions (5) on the interface $\Gamma$ and (15), for the second term in the left-hand side of (44), it holds, for sufficiently small $\Delta t$,

$$\Delta t \sum_{h=0}^{n-1} \left( \frac{u_1^{h+1} - u_1^h}{\Delta t}, p_1^h \right)_{L^2(\Gamma)} \simeq \int_\Gamma \int_0^{t_n} \dot{u}_1(\mathbf{x}, t) p_1(\mathbf{x}, t) \, dt \, d\gamma_{\mathbf{x}} = \mu_1 \mathcal{E}_{\Omega_1}(u_1, t_n),$$
(45)

Hence, we can write

$$\Delta t \sum_{h=0}^{n-1} \left( \frac{u_1^{h+1} - u_1^h}{\Delta t}, p_1^h \right)_{L^2(\Gamma)} = \mu_1 \mathcal{E}_1^n \geq 0$$
(46)

and finally from (44) to (46),

$$\mu_2 (1 - \Delta t) \mathcal{E}_2^n + \mu_1 \mathcal{E}_1^n \leq \mu_2 \Delta t \sum_{h=0}^{n-1} \mathcal{E}_2^h + \mu_2 c_2^2 \frac{\Delta t}{2} \sum_{h=0}^{n-1} \| F_h \|^2.$$
(47)

For the discrete energy in the subdomain $\Omega_2$, we obtain, under the natural assumption $\Delta t < 1$,

$$\mathcal{E}_2^n \leq \frac{\Delta t}{1 - \Delta t} \sum_{h=0}^{n-1} \mathcal{E}_2^h + \frac{c_2^2 \Delta t}{2(1 - \Delta t)} \sum_{h=0}^{n-1} \| F_h \|^2$$
(48)

and applying at last the discrete Gronwall's Lemma [23], we deduce, for every time instant $t_n$, the following upper bound:

$$\mathcal{E}_2^n \le \frac{c_2^2 \, \Delta t}{2(1 - \Delta t)} \sum_{h=0}^{n-1} \| F_h \|^2 \, \exp\left(\frac{t_n}{1 - \Delta t}\right). \tag{49}$$

If we finally consider the discrete energy in the subdomain $\Omega_1$, from (47), we can write

$$\mathcal{E}_1^n \le \frac{\mu_2}{\mu_1} \Delta t \left[\sum_{h=0}^{n-1} \mathcal{E}_2^h + \frac{c_2^2}{2} \sum_{h=0}^{n-1} \| F_h \|^2 \right] \tag{50}$$

and using (49) to bound from above every term in the first sum on the right-hand side of (50), we succeed in proving a complete stability result for our numerical scheme.

## 6. EXTENSIONS OF THE MODEL PROBLEM

The model problem described in Section 2 has been selected to formally analyse the stability of the corresponding energetic discretization without having to introduce a heavy notation. Numerical results reported in the next section will confirm the proposed theory.

Anyway, together with benchmarks related to (1)–(5), we will also treat more general test problems on both bounded and unbounded domains. In particular, a Neumann boundary condition $p_1(\mathbf{x}, t) = \bar{p}_1(\mathbf{x}, t)$ will be assigned on a portion $\Gamma_{1,N}$ of the boundary of the subdomain $\Omega_1$. In this case, we will consider also the usual *traction* BIE on that part of the boundary, that is,

$$\frac{1}{2} \bar{p}_1(\mathbf{x}, t) = K^* p_1(\mathbf{x}, t) - \mu_1 \, D u_1(\mathbf{x}, t), \tag{51}$$

where

$$K^* p_1(\mathbf{x}, t) = -\int_{\Gamma_{1,N}} \frac{1}{4\pi r} H[t - \frac{r}{c_1}] \frac{\partial r}{\partial \mathbf{n_x}} \left[\frac{\dot{p}_1(\boldsymbol{\xi}, t - \frac{r}{c_1})}{c_1} + \frac{p_1(\boldsymbol{\xi}, t - \frac{r}{c_1})}{r}\right] d\gamma_{\boldsymbol{\xi}}, \tag{52}$$

and

$$
\begin{aligned}
D u_1(\mathbf{x}, t) = -\int_{\Gamma_{1,N}} \frac{1}{4\pi r} H[t - \frac{r}{c_1}] &\left\{\frac{\partial^2 r}{\partial \mathbf{n_x} \partial \mathbf{n_\xi}} \left[\frac{\dot{u}_1(\boldsymbol{\xi}, t - \frac{r}{c_1})}{c_1} + \frac{u_1(\boldsymbol{\xi}, t - \frac{r}{c_1})}{r}\right]\right. \\
&\left. - \frac{\partial r}{\partial \mathbf{n_x}} \frac{\partial r}{\partial \mathbf{n_\xi}} \left[\frac{\ddot{u}_1(\boldsymbol{\xi}, t - \frac{r}{c_1})}{c_1^2} + \frac{2 \dot{u}_1(\boldsymbol{\xi}, t - \frac{r}{c_1})}{r c_1} + \frac{2 u_1(\boldsymbol{\xi}, t - \frac{r}{c_1})}{r^2}\right]\right\} d\gamma_{\boldsymbol{\xi}}.
\end{aligned}
\tag{53}
$$

Taking into account the nature of Equation (51) and having set $< \cdot, \cdot >_{\Gamma_{1,N}} = < \cdot, \cdot >_{L^2([0,T] \times \Gamma_{1,N})}$, the energetic weak formulation of the coupled problem will be

$$
\begin{cases}
< K^* p_1, \dot{v}_1 >_{\Gamma_{1,N}} - \mu_1 < D u_1, \dot{v}_1 >_{\Gamma_{1,N}} = \frac{1}{2} < \bar{p}_1, \dot{v}_1 >_{\Gamma_{1,N}}, & \forall v_1 \in H^1([0,T]; H^{\frac{1}{2}}(\Gamma_{1,N})) \\[2mm]
\frac{1}{\mu_1} < V \dot{p}_1, q_1 > - < K \dot{u}_{2|\Gamma}, q_1 > - \frac{1}{2} < \dot{u}_{2|\Gamma}, q_1 > = 0, & \forall q_1 \in L^2([0,T]; H^{-\frac{1}{2}}(\Gamma)) \\[2mm]
\mu_2 \mathcal{A}(u_2, v_2) + < p_1, \dot{v}_{2|\Gamma} > = -\mu_2 \mathcal{F}(v_2) + < \bar{p}, \dot{v}_{2|\Gamma_N} >_{\Gamma_N}, & \forall v_2 \in H^1([0,T]; H^1(\Omega_2))
\end{cases}
\tag{54}
$$

in the unknowns:

$$u_1 \in H^1([0,T]; H^{\frac{1}{2}}(\Gamma_{1,N})), \, p_1 \in L^2([0,T]; H^{-\frac{1}{2}}(\Gamma)) \text{ and } u_2 \in H^1([0,T]; H^1(\Omega_2)).$$

In this context, the choice (24) for the time approximation of $u_i$, $i = 1, 2$ is no longer optimal, because the cut-off property of the matrix part related to the discretization of the operator $D$ does not hold anymore.

Instead, it is expedient to consider, for $k = 0, \cdots, N_{\Delta t} - 1$, the following hat-shaped time shape function

$$\hat{\psi}_k(t) = R(t - t_k) - 2 R(t - t_{k+1}) + R(t - t_{k+2}),\tag{55}$$

which preserves the cut-off property of all BEM matrix blocks related to the unknown $u_1$; hence, in particular, as proved in [21], of the elements coming from the discretization of $< D u_1, \dot{v}_1 >_{\Gamma_{1,N}}$, which, after a regularizing procedure of the hypersingular bilinear form [24, 25] and an analytical integration in time, are of the form

$$-\frac{1}{4\pi(\Delta t)^2} \sum_{\alpha,\beta,\lambda=0}^{1} (-1)^{\alpha+\beta+\lambda} \int_{\Gamma_{1,N}} \int_{\Gamma_{1,N}} \frac{1}{r} H[\Delta_{h+\alpha,k+\beta+\lambda} - \frac{r}{c_1}] \mathcal{D}(r, \Delta_{h+\alpha,k+\beta+\lambda}) \, d\gamma_{\boldsymbol{\xi}} \, d\gamma_{\mathbf{x}},$$
$$\tag{56}$$

where

$$\mathcal{D}(r, \Delta_{hk}) = \frac{\mathbf{n_{\boldsymbol{\xi}}} \cdot \mathbf{n_{\mathbf{x}}}}{c_1^2} \hat{\varphi}_j|_{\Gamma_{1,N}}(\boldsymbol{\xi}) \hat{\varphi}_i|_{\Gamma_{1,N}}(\mathbf{x}) + \frac{1}{2}\left(\Delta_{hk} - \frac{r}{c_1}\right)^2 [\mathbf{n_{\boldsymbol{\xi}}} \times \nabla \hat{\varphi}_j|_{\Gamma_{1,N}}(\boldsymbol{\xi})] \cdot [\mathbf{n_{\mathbf{x}}} \times \nabla \hat{\varphi}_i|_{\Gamma_{1,N}}(\mathbf{x})].$$
$$\tag{57}$$

Matrix elements coming from the discretization of $< K^* p_1, \dot{v}_1 >_{\Gamma_{1,N}}$ have an expression similar to (32). In any case, we are still in presence of space singularities of type $O(r^{-1})$ as $r \to 0$.

## 7. NUMERICAL RESULTS

To validate the proposed energetic approach, we address some numerical examples obtained implementing the energetic weak formulation (20) and its extensions, in order to account also for bounded domains or situations in which the boundary of the unbounded subdomain $\Omega_1$ does not contain only the interface $\Gamma$, as described in the previous section.

The mesh of the analysis domain has been created with the code GMSH [26]. Linear four-node tetrahedra and linear three-node triangles have been employed for the FEM and BEM subdomains, respectively. In the current version, a strong coupling has been enforced, in the sense that the interface mesh between the two subdomains is conformal, that is, triangles for $\Gamma$ coincide with faces of the tetrahedra for $\Omega_2$, as well as the time–space interpolation adopted.

Several critical issues deserve some comments. The matrix elements coming from the BEM part of the coupling are computed as described in [20, 21]. In particular, time integrals are performed analytically obtaining, as already said, formulas (31) and (32)–(56). The resulting double space integrals contain only weak $O(r^{-1})$ singularities and are evaluated as follows. The outer space integral over the source element is performed numerically. A Gauss–Hammer rule with seven nodes has been employed, even if a faster rule with three nodes typically yields very accurate overall results. On the contrary, the inner integral is evaluated analytically if the projection of the source point on the plane of the field element is close to the element itself; otherwise, the wave front is approximated numerically using standard interpolation procedures and a fully numerical integration based on Gauss–Hammer quadrature rule with seven nodes is employed. The choices of the number of quadrature nodes has been done on the basis of the accurate analysis on this issue performed in [21].

The energetic BEM–FEM coupling requires, at every time step, the solution of the linear system (30) whose matrix $\mathbb{E}^{(0)}$ is nonsymmetric but highly sparse. Among the various efficient commercial tools apt to address this task, we have here selected the Pardiso code [27].

We remark that also the contributions $\mathbb{E}^{(k)}$ coming from the discretization of the convolution integrals are sparse and are stored either in memory or on the disk with a sparse format stocking. These simple provisions considerably reduce the cost of the time convolution and allow for the simulation of rather large-scale problems. The issue associated with the time consuming evaluation of double space integrals has been here mitigated by resorting to an OpenMP parallelization on shared memory architectures, although different strategies, including, for example, fast approaches, are under consideration.
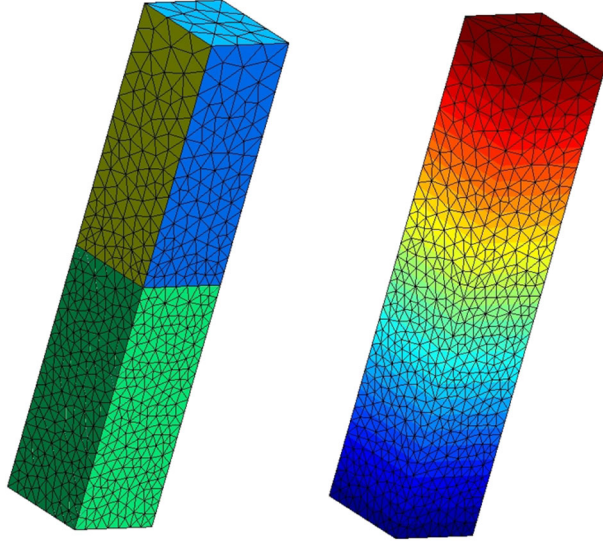
Figure 2. Meshes employed for example 1 and pressure chart at time $t = 40$.

### 7.1. Bar under tension

We first consider the classical benchmark (see for instance [25]) of a bar of height equal to 10 and square cross section with side equal to 2. On the lower surface, the Dirichlet boundary data $\bar{u} = 0$ is enforced, whereas the upper surface is subjected to a uniform Neumann condition $\bar{p} = H[t]$. On the lateral surface, $\bar{p} = 0$ is assumed. Here, we fix $\mu_1 = \mu_2 = 1$ and $c_1 = c_2 = 1$, together with $f_2(\mathbf{x}, t) = 0$.

The lower half $\Omega_2$ (FEM subdomain) has been discretized with tetrahedra imposing a uniform mesh size $\Delta x = 0.25$ (average length of element sides). The upper part $\Omega_1$ is modelled using the BEM, and the surface mesh is coarsened, from the interface to the bar top, by imposing a mesh size $\Delta x = 0.5$ on the upper surface. The time interval of the analysis has been set to $[0, 200]$, and different time steps have been tested, as clarified in the sequel. Figure 2 presents the mesh employed and the pressure distribution on the surface at time $t = 40$.

This benchmark is well known to be extremely challenging for standard BEM analysis in terms of stability properties when the time step decreases below a certain threshold. In [20], these issues have been solved using a pure BEM energetic formulation and the same robust and stable behaviour appears to be preserved also in the current energetic coupling with FEM. Indeed, in Figures 3–5, we collect the plots for pressure (at a point on the upper surface and at the interface) and tractions (at a point of the interface) using largely different time steps. No instabilities can be observed and no spurious wave reflections are produced at the discretized interface.

### 7.2. Spherical cavity in an unbounded domain

As a second benchmark, we consider a spherical cavity of radius $R_C = 3$ embedded in an infinite linear and homogeneous medium. The $\Omega_2$ region is defined by $R_C \leq r \leq R_I$, with $R_I = 5$, and the interface $\Gamma$ is the spherical surface with radius $r = R_I$. Here, $\mu_1 = \mu_2 = 1$ and $f_2(\mathbf{x}, t) = 0$.

The mesh adopted is depicted in Figure 6 and has an average side length $\Delta x = 0.5$ and $\Delta x = 1$ on the inner surface and on the interface, respectively. In a first set of analyses, where $c_1 = c_2 = 1$, the inner surface is subjected to a uniform traction $\bar{p} = H[t]$. The analytical solution is endowed with spherical symmetry and can be obtained following the same scheme as in [20], obtaining

$$u(r) = \frac{R_C^2}{r}\left(1 - e^{(r-R_C-t)/R_C}\right), \qquad t > r - R_C \tag{58}$$

$$p(r) = e^{(r-R_C-t)/R_C}\left(\frac{R_C^2}{r^2} - \frac{R_C}{r}\right) - \frac{R_C^2}{r^2}, \quad t > r - R_C. \tag{59}$$
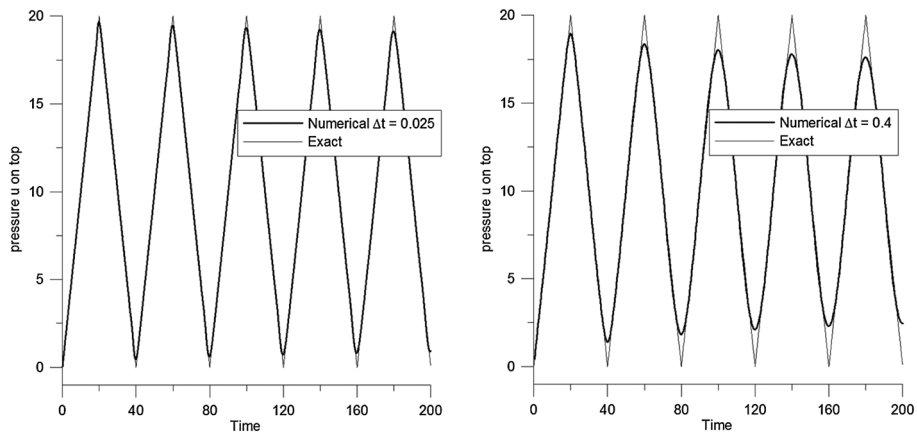
Figure 3. Example 1. Pressure evolution at bar-top for different time steps.
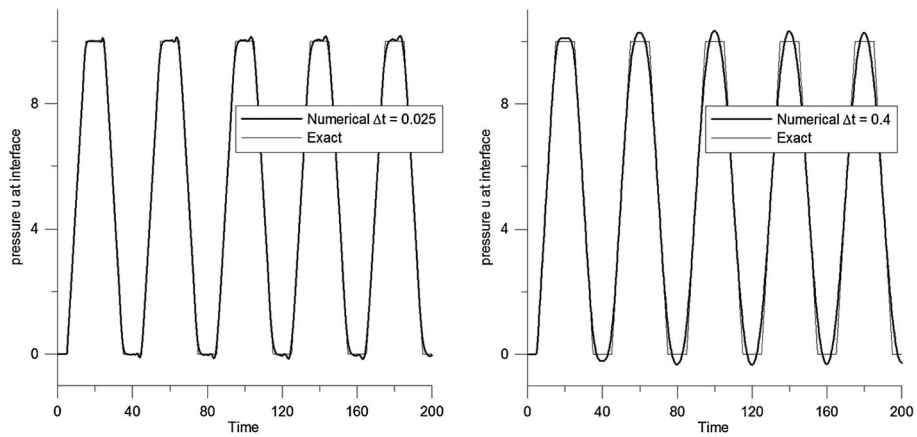


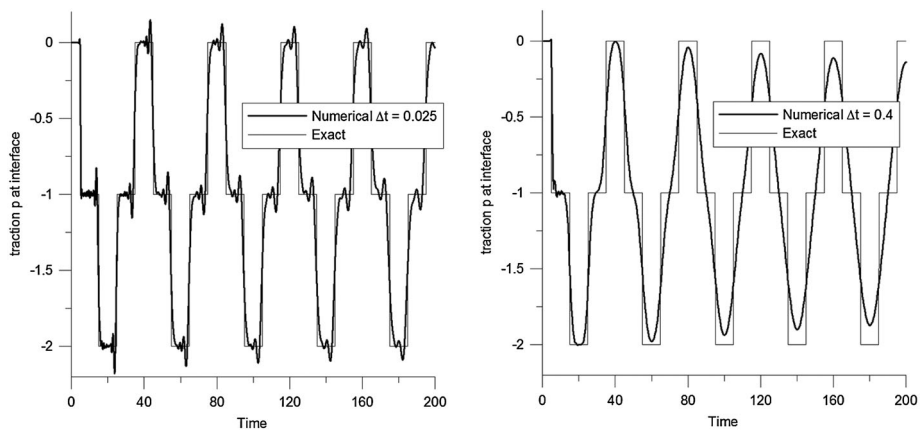Figure 4. Example 1. Pressure evolution at interface for different time steps.



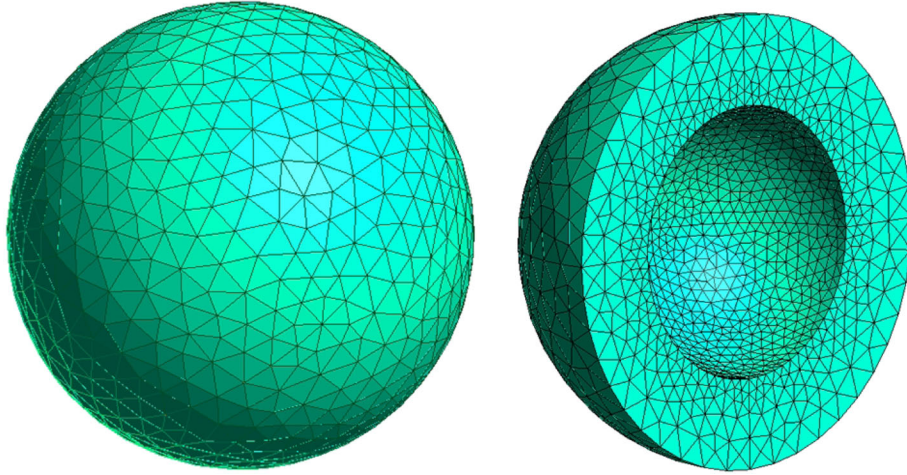Figure 5. Example 1. Traction evolution at interface for different time steps.
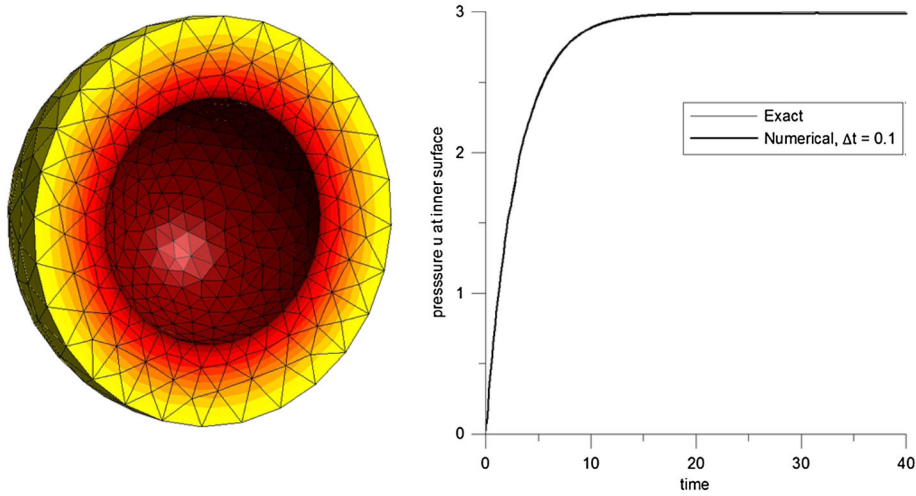
Figure 6. Mesh adopted for example 2.



Figure 7. Example 2. Chart of pressure distribution and time history for pressure at inner radius.

A spherical wave travels with unit speed from the inner surface towards infinity and traverses the interface at time $t = R_I - R_C$. The time interval of the analysis has been set to $[0, 40]$. Figure 7 presents the pressure chart at the end of the analysis and the pressure history at a point of the inner surface.

In Figure 8, on the contrary, the time histories of the tractions at the interface for a broad range of time steps are collected. Also, in this case, no reflections are observed, and even if the traction history presents some oscillations for small $\Delta t$, these never explode into instabilities. In this specific example, the boundary elements placed on the interface act as an absorbing layer preventing waves from being reflected backwards. The effectiveness of the coupling procedure in this sense can be measured by comparing the present solution with the case of a finite domain with no absorbing conditions (see, e.g. [20]). In this latter situation, a train of waves keep travelling and bouncing between the inner and outer surface; these reflections are on the contrary virtually absent in the example analysed herein, independently of the time step adopted.

Further, in Figure 9, we have reported the approximate solution at inner radius $r = R_C$, fixing different velocities in the two subdomains: we deduce that until the perturbation is inside $\Omega_2$, pressure behaves as in a monodomain with the physical constants of $\Omega_2$; then, when the wavefront has
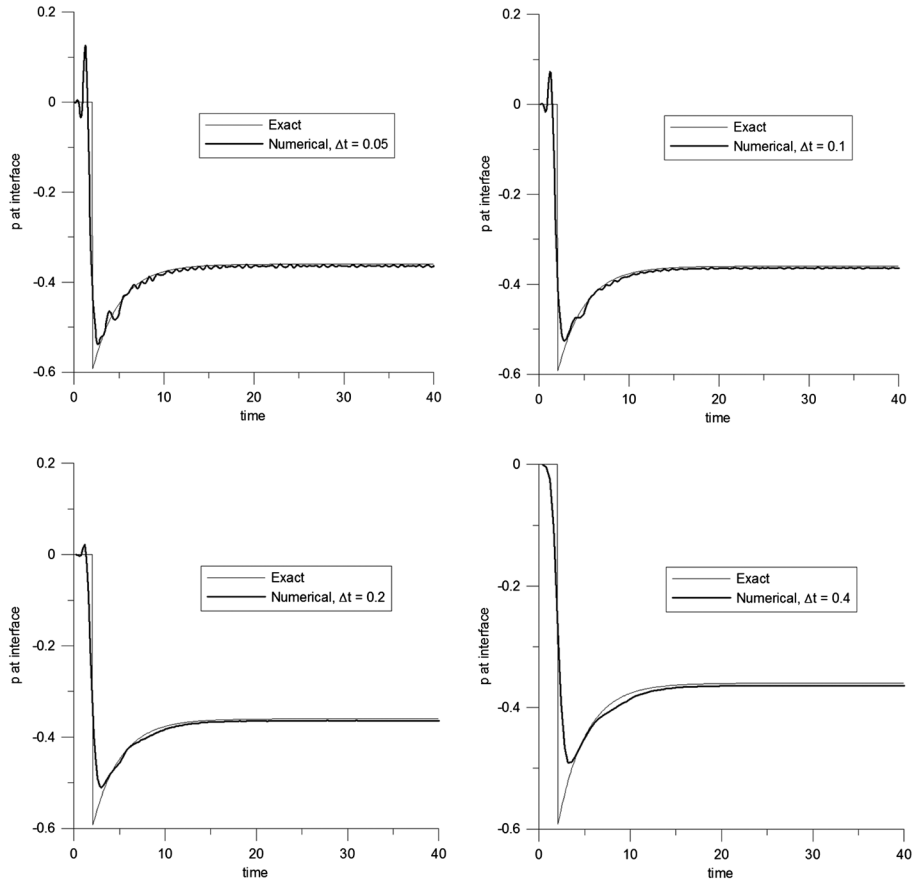
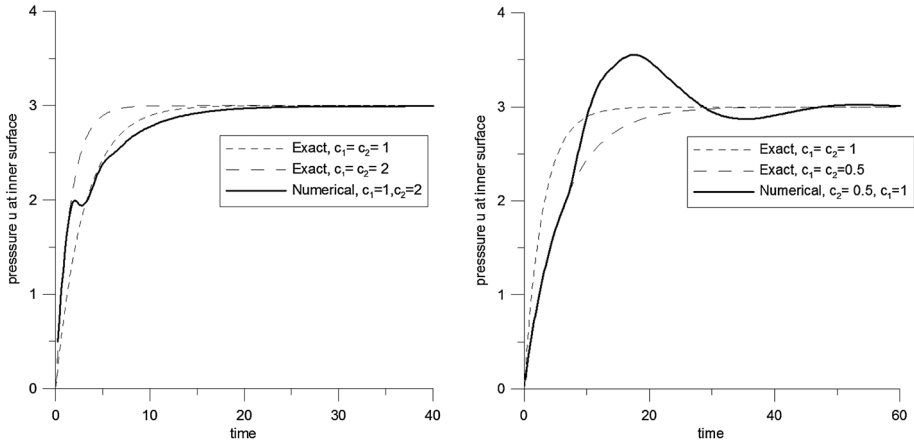Figure 8. Example 2. History of interface tractions for different time steps.



Figure 9. Example 2. Pressure history at inner radius for simulations on bidomains.

completely left the interface $\Gamma$, pressure tends to behave as in a monodomain with the physical constants of $\Omega_1$. For $c_1 = 1$, $c_2 = 2$, convergence is from below; for $c_1 = 1$, $c_2 = 0.5$, the approximate solution converges oscillating.

All the obtained numerical results are similar to those found in [19], for an analogous exterior 2D bidomain, using an energetic BEM–BEM coupling.
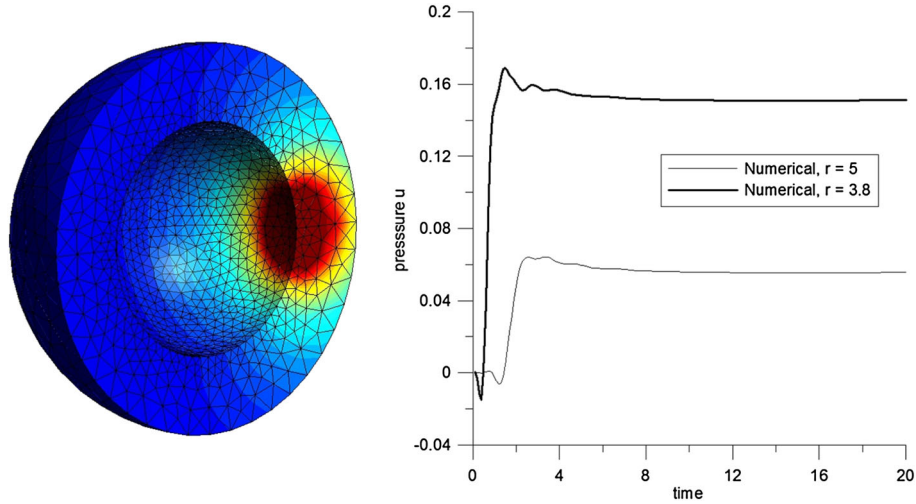
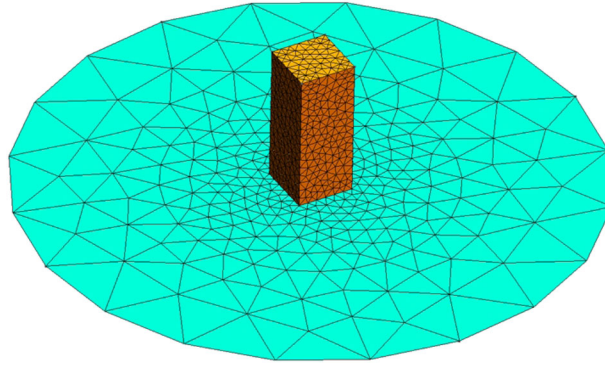Figure 10. Example 2. Pressure history due to a point source.



Figure 11. Example 3. Column on a half-space; mesh adopted.

In order to test the performance of the proposed formulation in a more general setting, where, differently from previous examples, waves impinge on the interface also at oblique angles, a second set of analyses is run assuming a different loading. A point source of intensity $H[t]$ is applied to a node of the inner surface, whereas $\bar{p} = 0$ elsewhere at $r = R_C$. Here, we fix $\mu_1 = \mu_2 = 1$ and $c_1 = c_2 = 1$. In Figure 10, we plot the pressure distribution at the end of the analysis $T = 20$, whereas on the right the time history of pressure at the points of the surfaces $r = 3.8$ and $r = 5$, at the minimum distance from the source. Also, in this case, no spurious reflections can be observed.

### 7.3. Column resting on a half space

The formulation developed and implemented in this work employs the fundamental solution for the unbounded space (7) and cannot be applied as it is to problems where a finite domain rests on a half-space. However, this type of simulation is the greatest interest, especially in view of its applications to problems in seismology (see, e.g. [17]). As well known, however, a simple provision allows to address also this situation, as depicted in Figure 11, where a column modelled by FEM rests on a semi-infinite space. Together with the interface, also a portion of the free surface of the infinite domain has to be modelled by BEM, and on the BEM nodes, where the mesh is truncated, the condition $\bar{u} = 0$ is enforced. The strategy is very robust and a little sensitive to the truncation distance and to the size of the elements employed on the free surface.
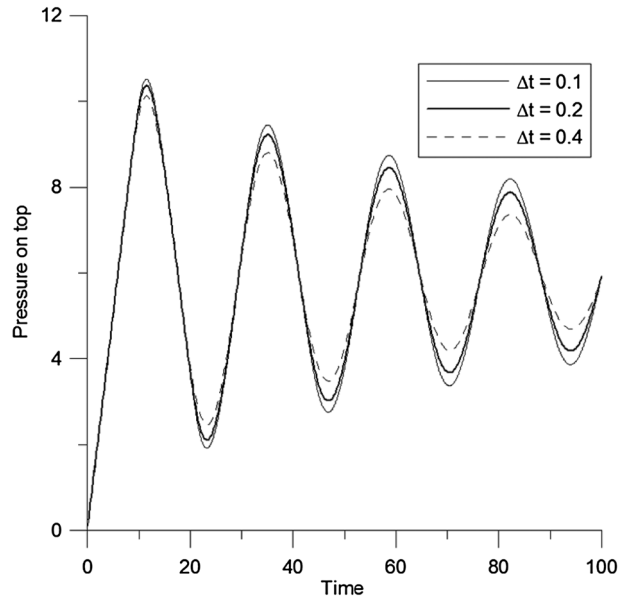
Figure 12. Example 3. Pressure history at a point on the top surface of the column.

In the specific case here analysed, the bar has a height equal to 5 and a square cross section with a side equal to 2. The truncation distance has been set equal to 10. The upper surface is subjected to a uniform Neumann condition $\bar{p} = H[t]$, whereas on the lateral surface and on the BEM surface, $\bar{p} = 0$ is assumed. We also fix unitary parameters and velocities and trivial source terms. The time interval of the analysis has been set to [0, 100], that is, much larger than the time of travel of possible reflected waves from the artificial truncation line of the surface mesh. However, no spurious reflection can be appreciated, and the maximum amplitude of the pressure on the column upper surface, depicted in Figure 12, slowly and smoothly decreases as a result of the energy dissipation of waves radiating to infinity.

## 8. CONCLUSIONS AND PERSPECTIVES

A novel BEM–FEM coupling procedure has been proposed, resting on a recently developed energetic BEM formulation. A model problem of wave propagation in an unbounded domain has been analysed first; after discussing the discretization strategy adopted, the stability of the numerical scheme has been proved. A fully three-dimensional implementation has been developed in a more general context, also allowing for the analysis of bounded domains. All the presented numerical results have confirmed the excellent stability properties of the adopted coupling scheme, even in the most challenging benchmarks.

In particular, the proposed coupling strategy can be seen as an accurate form of 'ABC' for problems in dynamics defined on unbounded domains and discretized via a classical domain technique such as the FEM. Indeed, in all the performed numerical tests, artificial waves reflected at the interface are virtually absent for a broad range of time steps employed in the time integration and of mesh refinement levels.

In this paper, only strong coupling and conformal meshes have been considered. In order to exploit the higher accuracy of the BEM, one should relax the interface conditions and introduce weak time–space coupling conditions, which are currently under investigation.

To make the methodology applicable to truly large-scale problems, special care should be also devoted to numerical issues concerning computing time in order to speed up the evaluation of multiple surface integrals and of the time convolution. One of the first approaches for a fast evaluation of the retarded potentials related to scattering problems was published in [28], employing a plane

wave expansion of the respective integral kernel. This idea was later extended to elastodynamics in [29]. An alternative methodology, which also extends the time domain formulations to problems where the time domain fundamental solution is not known, is the so-called convolution quadrature method based BEM [30], recently investigated also in [11]. The analysis of these and alternative options will be the topic of future research.

## REFERENCES

1. Antes H, Beer G, Moser W. Soil-structure interaction and wave propagation problems in 2D by a Duhamel integral based approach and the convolution quadrature method. *Computer Mechanics* 2005; **36**(6):431–443.
2. Ha Duong T, Ludwig B, Terrasse I. A Galerkin BEM for transient acoustic scattering by an absorbing obstacle. *International Journal for Numerical Methods in Engineering* 2003; **57**:1845–1882.
3. Buffa A, Costabel M, Schwab C. Boundary elements methods for Maxwell's equation on non-smooth domains. *Numerical Mathematics* 2002; **92**(4):679–710.
4. Sari M, Demir I. Wave modelling through layered media using the BEM. *Journal of Applied Sciences* 2006; **6**(8):1703–1711.
5. Almeida V. S, de Paiva J. B. Static analysis of soil/pile interaction in layered soil by BEM/BEM coupling. *Advances in Engineering Software* 2007; **38**:835–845.
6. Frangi A, Maier G. Dynamic elastic-plastic analysis by a symmetric Galerkin boundary element method with time-independent kernels. *Computer Methods in Applied Mechanics and Engineering* 1999; **171**:281–308.
7. Frangi A, Novati G. BEM–FEM coupling for 3D fracture mechanics applications. *Computer Mechanics* 2003; **32**:415–422.
8. Czygan O, von Estorff O. Fluid-structure interaction by coupling BEM and nonlinear FEM. *Engineering Analysis with Boundary Elements* 2002; **26**:773–779.
9. Wegner JL, Yao MM, Zhang X. Dynamic wave–soil–structure interaction analysis in time domain. *Computer and Structures* 2005; **83**:2206–2214.
10. Rabinovich D, Givoli D, Becache E. Comparison of high-order absorbing boundary conditions and perfectly matched layers in the frequency domain. *International Journal for Numerical Methods in Engineering* 2010; **26**:1351–1369.
11. Falletta S, Monegato G. An exact non reflecting boundary condition for 2D time-dependent wave equation problems. *Wave Motion* 2013. DOI: 10.1016/j.wavemoti.2013.06.001, in press.
12. Mansur WJ, Yu G, Carrer JAM, Lie ST, Siqueira EFN. The $\theta$ scheme for time domain BEM/FEM coupling applied to the 2-D scalar wave equation. *Communications in Numerical Methods in Engineering* 2000; **16**(6):439–448.
13. Lie ST, Yu GY. Stability improvement to BEM/FEM coupling scheme for 2D scalar wave problems. *Advances in Engineering Software* 2002; **33**:17–26.
14. Yu GY. A symmetric BEM/FEM coupling procedure for 2-D elastodynamic problems. *Journal of Applied Mechanics* 2003; **70**:451–454.
15. Ruberg T, Schanz M. Coupling finite and boundary element methods for static and dynamic elastic problems with non-conforming interfaces. *Computer Methods in Applied Mechanics and Engineering* 2008; **198**:449–458.
16. Abboud T, Joly P, Rodriguez J, Terrasse I. Coupling discontinuous Galerkin methods and retarded potentials for transient wave propagation in unbounded domains. *Journal of Computational Physics* 2011; **230**(15):5877–5907.
17. von Estorff O, Hagen H. Iterative coupling of FEM and BEM in 3D transient elastodynamics. *Engineering Analysis with Boundary Elements* 2005; **29**:775–787.
18. Aimi A, Diligenti M. A new space–time energetic formulation for wave propagation analysis in layered media by BEMs. *International Journal for Numerical Methods in Engineering* 2008; **75**:1102–1132.
19. Aimi A, Gazzola S, Guardasoni C. Energetic boundary element method analysis of wave propagation in 2D multilayered media. *Mathematical Methods in the Applied Sciences* 2012; **35**:1140–1160.
20. Aimi A, Diligenti M, Frangi A, Guardasoni C. A stable 3D energetic Galerkin BEM approach for wave propagation interior problems. *Engineering Analysis with Boundary Elements* 2012; **36**:1756–1765.
21. Aimi A, Diligenti M, Frangi A, Guardasoni C. Neumann exterior wave propagation problems: computational aspects of 3D energetic Galerkin BEM. *Computer Mechanics* 2013; **51**:475–493.
22. Frangi A. Causal shape functions in the time domain boundary element method. *Computer Mechanics* 2000; **25**:533–541.
23. Quarteroni A, Valli A. *Numerical Approximation of Partial Differential Equations*. Springer-Verlag: Berlin, 1994.
24. Aimi A, Panizzi S. On the regularization of bilinear forms with hypersingular kernel. *Applied Mathematics and Computation* 2013. in press.
25. Frangi A. Elastodynamics by BEM: a new direct formulation. *International Journal for Numerical Methods in Engineering* 1999; **45**:721–740.
26. Geuzaine C, Remacle JF. Gmsh: a three-dimensional finite element mesh generator with built-in pre- and post-processing facilities. *International Journal for Numerical Methods in Engineering* 2009; **79**:1309–1331.
27. Schenk O, Gartner K. PARDISO User Guide Version 4.1.2, 2011. (Available from: http://www.pardiso-project.org).
28. Ergin AA, Shanker B, Michielssen E. Fast evaluation of three-dimensional transient wave fields using diagonal translation operators. *Journal of Computational Physics* 1998; **146**:157–180.

29. Takahashi T, Nishimura N, Kobayashi S. A fast BIEM for three-dimensional elastodynamics in time domain. *Engineering Analysis with Boundary Elements* 2003; **27**:491–506.
30. Schanz M, Antes H. Application of operational quadrature methods in time domain boundary element methods. *Mechanica* 1997; **32**:179–186.